Plasma Phys. Control. Fusion **53** (2011) 054003 (14pp) doi:10.1088/0741-3335/53/5/054003

Turbulence simulations of barrier relaxations and transport in the presence of magnetic islands at the tokamak edge

P Beyer[1], F de Solminihac[1], M Leconte[2], X Garbet[3], F L Waelbroeck[4], A I Smolyakov[5] and S Benkadda[1]

[1] International Institute for Fusion Science, CNRS – Université de Provence, Centre de St. Jérôme, Case 321, 13397 Marseille Cedex 20, France
[2] WCI Center for Fusion Theory, NFRI, Research Bdg #2, 113 Gwahangno, Yuseong-gu, Daejeon, 305-333, Korea
[3] Association Euratom–CEA, CEA/DSM/IRFM, Centre de Cadarache, 13108 St Paul-Lez-Durance, France
[4] Institute for Fusion Studies, The University of Texas, Austin, TX 78712-0262, USA
[5] Department of Physics and Engineering Physics, University of Saskatchewan, 116 Science Place, Saskatoon, S7N 5E2, Canada

E-mail: peter.beyer@univ-provence.fr

Received 7 September 2010 , in final form 10 November 2010
Published 31 March 2011
Online at stacks.iop.org/PPCF/53/054003

Abstract
The control of transport barrier relaxation oscillations by resonant magnetic perturbations (RMPs) is investigated with three-dimensional turbulence simulations of the tokamak edge. It is shown that single harmonics RMPs (single magnetic island chains) stabilize barrier relaxations. In contrast to the control by multiple harmonics RMPs, these perturbations always lead to a degradation of the energy confinement. The convective energy flux associated with the non-axisymmetric plasma equilibrium in the presence of magnetic islands is found to play a key role in the erosion of the transport barrier that leads to the stabilization of the relaxations. This convective flux is studied numerically and analytically. In particular, it is shown that in the presence of a mean shear flow (generating the transport barrier), this convective flux is more important than the radial flux associated with the parallel diffusion along perturbed field lines.

1. Introduction

Transport barriers in tokamak plasmas are key ingredients of improved confinement regimes. These barriers are thin layers in which turbulent transport of heat and matter is reduced significantly and a strong pressure gradient builds up. At the plasma edge, the barrier typically

is not stable but exhibits relaxation oscillations associated with intermittent high energy flux peaks. These barrier relaxations are an essential characteristic of the so-called edge localized modes (ELMs) [1]. The control of such ELMs is a crucial issue for the next generation of tokamak experiments such as ITER. Experimental studies on a variety of different tokamaks such as DIII-D [2, 3], JET [4] and TEXTOR [5, 6] reveal that a qualitative control of ELMs can be obtained by imposing resonant magnetic perturbations (RMPs) at the plasma edge. Such a perturbation has the same helicity as the magnetic field line on a particular (resonant) magnetic surface, and leads to a perturbation of this surface by the formation of magnetic islands [7].

The control of ELMs by RMPs is generally attributed to a reduction in the pressure gradient by a radial energy flux associated with the strong collisional heat flux along perturbed field lines [8]. In particular, it has been found that when increasing the perturbation amplitude, ELMs' control becomes efficient when field line stochasticity appears, induced by overlapping magnetic islands [8]. However, the actual degree of magnetic island formation and stochasticity present in the plasma due to the applied magnetic field is an open question. Indeed, there is evidence from magnetohydrodynamical (MHD) modelling, that in rotating plasmas the generation of current perturbations near rational surfaces could prevent reconnection, leading to an effective screening of the magnetic perturbation [9, 10]. In addition, plasma response calculations show that magnetic islands are suppressed when the electron fluid is rotating past the perturbation [11, 12]. On DIII-D, observations show that the poloidal electron velocity reverses towards the top of the pedestal, so that the presence of a single penetrated magnetic island near the reversal point is consistent with theoretical expectations [12]. It is therefore interesting to investigate, whether a control of transport barrier relaxations can also be achieved with a single island chain. This problem is relevant to the efforts to reconcile the experimental observations of ELM suppression with the theoretical predictions of the screening of almost all the islands. In particular, we will study here the possible mechanisms that can lead to an increase in the radial energy flux in the presence of a magnetic island, as well as their relative importance. For this purpose, the magnetic perturbation is prescribed and the resulting transport is parametrized by the magnitude of this perturbation which remains a free parameter in our consideration.

In previous works, barrier relaxations have been studied by means of three-dimensional turbulence simulations [13, 14] and the possible control of these relaxations by externally induced RMPs has been investigated [15, 16]. In this framework, it has also been shown recently that a single harmonic RMP localized at the barrier position can also lead to a stabilization of the relaxations [17]. However, in this geometry, the confinement is always degraded.

As shown in these turbulence simulations, a key element for the stabilization of barrier relaxations is the convective energy flux associated with the non-axisymmetric plasma equilibrium in the presence of magnetic islands. In fact, when a magnetic island chain is externally imposed inside the plasma, the modified equilibrium pressure and electric potential give rise to a convective flux that plays an important role in the local erosion of the transport barrier and the stabilization of its relaxations. The magnetic island chain can either result from a single harmonic resonant perturbation [17] or from a multiple harmonic resonant perturbation leading to a complex geometry with stochastic regions and residual islands [15, 16]. In this work, we will characterize this convective flux. In particular, we will show that in the presence of a mean poloidal flow which is at the origin of the transport barrier, the convective flux is more important than the radial flux induced by the parallel diffusion.

The paper is organized as follows. In section 2, we present the turbulence model and briefly recall the numerical observations of transport barrier relaxations in this framework. In section 3, the numerical results on the control of these relaxations by multiple or single

harmonics RMPs are discussed. In particular, the essential role of the convective energy flux associated with the non-axisymmetric equilibrium is worked out. Section 4 is then devoted to the numerical and analytical characterization of the energy fluxes in the presence of a magnetic island. The conclusions are presented in section 5.

2. Turbulence model and transport barrier relaxations

2.1. Turbulence model

The three-dimensional turbulence model studied here consists of the normalized reduced MHD equations for the plasma pressure p and the electric potential ϕ [14],

$$\partial_t \nabla_\perp^2 \phi + \left\{\phi, \nabla_\perp^2 \phi\right\} = -\nabla_\parallel^2 \phi - \boldsymbol{G}\, p + \nu \nabla_\perp^4 \phi + \mu \nabla_\perp^2 \left(\phi_{\rm imp} - \bar{\phi}\right), \tag{1}$$

$$\partial_t p + \{\phi, p\} = \delta_{\rm c} \boldsymbol{G}\, \phi + \chi_\parallel \nabla_\parallel^2 p + \chi_\perp \nabla_\perp^2 p + S. \tag{2}$$

In toroidal coordinates (r, θ, φ) and in a slab geometry (x, y, z) in the vicinity of a reference surface $r = r_0$ at the plasma edge, i.e. $x = (r - r_0)/\xi_{\rm bal}$, $y = r_0\theta/\xi_{\rm bal}$, $z = R_0\varphi/L_{\rm s}$, the normalized operators are

$$\nabla_\parallel = \partial_z + \left(\frac{\zeta}{q_0} - x\right)\partial_y - \{\psi_{\rm RMP}, \cdot\} \quad \text{with} \quad \zeta = \frac{L_{\rm s} r_0}{R_0 \xi_{\rm bal}},$$

$$\boldsymbol{G} = \sin\theta\, \partial_x + \cos\theta\, \partial_y, \qquad \nabla_\perp^2 = \partial_x^2 + \partial_y^2, \qquad \{\phi, \cdot\} = \partial_x \phi \partial_y - \partial_y \phi \partial_x,$$

where $\psi_{\rm RMP}$ represents the externally imposed perturbation of the poloidal magnetic flux (see section 3). Here, $q_0 = q(r_0)$ is the safety factor at the reference surface, R_0 is the major radius of the magnetic axis and $L_{\rm s}$ is the shear length used as the scale length in the direction parallel ($\parallel$) to the unperturbed magnetic field. The normalization length in the perpendicular ($\perp$) direction is the resistive ballooning length given by

$$\xi_{\rm bal} = \left(\frac{m_{\rm e}}{m_{\rm i}} \frac{q_0^2 R_0 \nu_{\rm e}}{c_{\rm s}}\right)^{\frac{1}{2}} \left(\frac{R_0}{L_{\rm p}}\right)^{\frac{1}{4}} \frac{L_{\rm s}}{q_0 R_0} \rho_{\rm s},$$

where $m_{\rm e}/m_{\rm i}$ is the ratio of the electron to the ion mass and $\nu_{\rm e}$, $c_{\rm s}$, $L_{\rm p}$, $\rho_{\rm s}$ are reference values of the electron collision frequency, the sound speed, the pressure gradient length and the ion Larmor radius at electron temperature, respectively. For a collisional tokamak plasma edge, one typically finds $\xi_{\rm bal} \sim \rho_{\rm s}$. Time is normalized to the interchange time

$$\tau_{\rm int} = \left(\frac{L_{\rm p} R_0}{2 c_{\rm s}^2}\right)^{\frac{1}{2}} = \left(\frac{R_0}{2 L_{\rm p}}\right)^{\frac{1}{2}} \frac{L_{\rm p}}{c_{\rm s}},$$

which typically is one order of magnitude larger than the characteristic inverse drift frequency $L_{\rm p}/c_{\rm s}$. Note that the transport mechanisms investigated in the following rely on the toroidal magnetic curvature that gives rise to the $\boldsymbol{G}$ operator in (1) and (2). As the magnetic curvature also triggers resistive ballooning turbulence, the resistive MHD equations provide a minimal model for studying the implications on turbulence and barrier dynamics of the transport associated with magnetic islands. The mechanisms investigated here therefore are present even if the precise character of the turbulence may be modified by additional physical effects, e.g. drift-Alfvén dynamics [18].

The perpendicular ion viscosity (ν) and heat conductivity ($\chi_\perp$) coefficients in (1) and (2) are normalized using the perpendicular scale length $\xi_{\rm bal}$, whereas the parallel heat conductivity coefficient $\chi_\parallel$ is normalized with the parallel scale length $L_{\rm s}$. In the present simulations, we use $\nu = \chi_\perp = 0.93$ and $\chi_\parallel = 1$. Note that $\chi_\perp$ is one order of magnitude lower than the normalized turbulent heat diffusivity $\chi_\perp^{\rm turb}$, when following a mixing

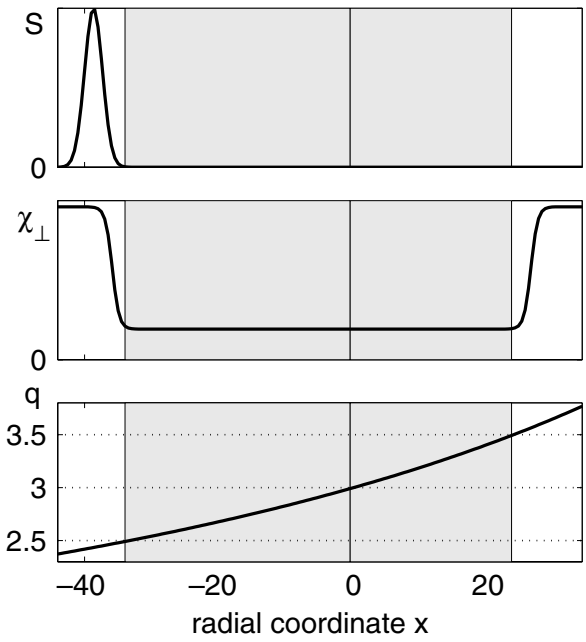

Figure 1. The energy source S (top), the perpendicular heat diffusivity $\chi_\perp$ (middle), and the safety factor q (bottom) as a function of the normalized radial coordinate x. The shaded region indicates the main computational domain between $q = 2.5$ and $q = 3.5$.

length estimate: $\chi_\perp^{\text{turb}} \sim \gamma_{\max}\sigma_r^2\tau_{\text{int}}/\xi_{\text{bal}}^2 \sim 10$. (The maximal growth rate $\gamma_{\max}$ of the resistive ballooning modes is one order of magnitude lower than the inverse interchange time, $\gamma_{\max} \sim 0.1/\tau_{\text{int}}$. The radial correlation length of the turbulence is of the order of the width σ_r of the Fourier components of the modes or even larger in case that signatures of the global mode structure are still present in the turbulence, roughly $\sigma_r \sim 10\xi_{\text{bal}}$ [19].) Note also that the ratio of $\chi_\parallel/\chi_\perp \sim 1$ of the normalized coefficients corresponds to a ratio of the dimensional coefficients of $L_{\text{s}}^2/\xi_{\text{bal}}^2 \sim 10^7$–$10^8$. Finally, $\delta_{\text{c}} = \frac{5}{3}\,2L_{\text{p}}/R_0$ is a curvature parameter set to $\delta_{\text{c}} = 0.01$.

In the present model, resistive ballooning turbulence is driven by an energy source S located close to the inner boundary of the main computational domain. The latter corresponds to the volume delimited by the toroidal surfaces characterized by $q = 2.5$ and $q = 3.5$, respectively, and including the reference surface $q = q_0 = 3$ (see figure 1). Here, a linear $1/q$ profile is assumed, and $\xi_{\text{bal}}/r_0 = 1/500$, $L_{\text{s}}/R_0 = 1$. The complete computational domain is slightly larger and delimited by $x_{\min} < x_{q=2.5}$ and $x_{\max} > x_{q=3.5}$. The source S gives rise to a constant incoming (from the plasma center into the main computational domain) energy flux, $Q_{\text{tot}} = \int_{x_{\min}}^{x_{q=2.5}} S\,\mathrm{d}x$. The pressure profile $\bar{p}(x,t) = \langle p\rangle_{y,z}$ evolves self-consistently according to the energy transport equation (the toroidal and poloidal average $\langle\cdot\rangle_{yz}$ of (2)),

$$\partial_t \bar{p} = -\partial_x\,(Q_{\text{conv}} + Q_{\text{coll}} + Q_{\delta B}) + S, \tag{3}$$

with $Q_{\text{conv}} = \langle p\,\partial_y\phi\rangle_{y,z}$, $Q_{\text{coll}} = -\chi_\perp\partial_x\bar{p}$, $Q_{\delta B} = -\chi_\parallel\langle\partial_y\psi_{\text{RMP}}\nabla_\parallel p\rangle_{y,z}$. In a statistically stationary state, averaging (3) in time and integrating in the radial direction leads to the energy flux balance

$$Q_{\text{conv}}(x) + Q_{\text{coll}}(x) + Q_{\delta B}(x) = Q_{\text{tot}} \qquad \text{for} \quad x \geqslant x_{\text{q=2.5}}. \tag{4}$$

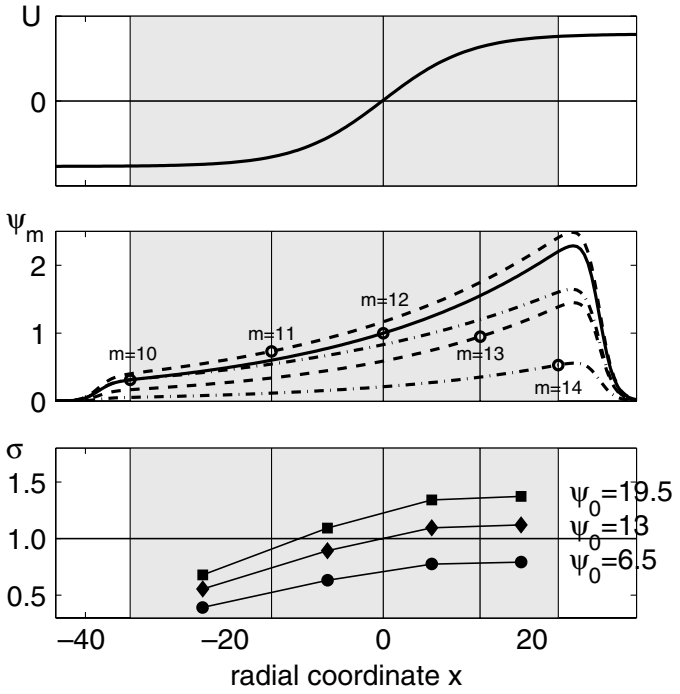

Figure 2. Imposed rotation velocity U (top) and amplitudes ψ_m of the different harmonics of the prescribed poloidal magnetic flux perturbation (middle), as a function of the normalized radial coordinate x. Circles indicate the amplitudes ψ_m on the corresponding resonant surfaces $q = m/n_0$. The bottom panel shows the Chirikov parameter deduced from these amplitudes for the different values of ψ_0 used in the following.

2.2. Transport barrier relaxations

When a poloidal $E \times B$ flow $U\boldsymbol{e}_y = \mathrm{d}_x\phi_{\mathrm{imp}}\boldsymbol{e}_y$ with radially localized velocity shear is imposed via the last term in (1) (with friction coefficient μ, and $\bar{\phi} = \langle\phi\rangle_{y,z}$), the turbulent radial energy flux Q_{conv} is reduced in the velocity shear region. According to the flux balance (4), when no magnetic perturbation is present ($\psi_{\mathrm{RMP}} = 0 \Rightarrow Q_{\delta B} = 0$), the pressure gradient steepens in the shear layer, i.e. a transport barrier forms [20]. Note that the forced poloidal rotation U is artificial. However, there exists actually no turbulence simulation reproducing self-consistently the generation of a transport barrier. As our purpose here is not to describe a self-consistent H-mode but rather to study the transport mechanisms associated with magnetic islands in the presence of a transport barrier, we generate the latter in our model via the imposed flow. Figure 2 (top) shows the profile of the rotation velocity $U = \omega_E d \tanh(x/d)$ used in the present simulations. The shear is maximal $\max(\mathrm{d}_x U) = \omega_E$ at the reference surface $q = 3$ leading to a transport barrier at that position. The parameter d characterizes the width of the velocity shear layer. Typically, such barrier is not stable but exhibits relaxation oscillations [13, 14]. Time traces of the convective flux Q_{conv} at the barrier center and the edge energy confinement time $\int \bar{p}\,\mathrm{d}x/Q_{\mathrm{tot}}$ are shown in figure 3 (left, top) and (right), respectively. Quasi-periodic relaxations of the transport barrier are characterized by drops in the energy confinement time associated with strong flux peaks.

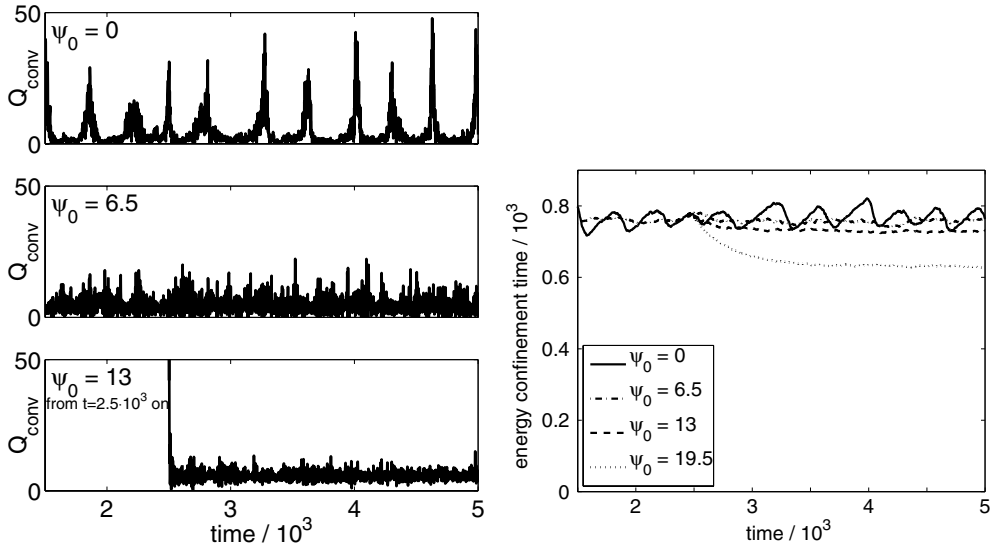

Figure 3. Time evolutions of the convective flux Q_{conv} at the barrier center $x = 0$, $q = 3$ (left) and of the edge energy confinement time (right) for different amplitudes ψ_0 of the multiple harmonics magnetic perturbation (5). Here, $Q_{\mathrm{tot}} = 10$, $\omega_E = 6$, $d = 11.7 = 0.15(x_{\max} - x_{\min})$.

3. Effect of RMPs on barrier dynamics

3.1. Multiple harmonics perturbation

In the electrostatic model (1), (2), we now impose a static RMP described by the normalized poloidal magnetic flux

$$\psi_{\mathrm{RMP}}^{\mathrm{multiple}} = \psi_0 \sum_m (-1)^m \psi_m(x) \cos(m\theta - n_0\varphi) \tag{5}$$

$$\text{with} \quad \psi_m(x) = C \frac{\sin\left[(m - m_0)\,\frac{\Delta\theta_c}{2\beta_1}\right]}{m\,(m - m_0)\,\pi} \exp\left[\frac{m}{\beta_1 r_c}\,(r_0 + \xi_{\mathrm{bal}} x - r_c)\right] .$$

Here, $(m_0, n_0) = (12, 4)$, $\Delta\theta_c = 2\pi/5$, $\beta_1 = 0.6$ and $r_c/\xi_{\mathrm{bal}} = 590$ are parameters typical for the DED device in the TEXTOR tokamak [21, 22] and the constant C is chosen such that $\psi_{m_0}(x = 0) = 1$. The radial profiles of the amplitudes $\psi_m(x)$ are shown in figure 2 (middle) for the five harmonics that are resonant in the main computational domain. Note that the amplitude of each harmonic m is increasing with radius but that the size of the magnetic island induced by each harmonic m is determined by its amplitude at the corresponding resonant surface $q(x) = m/n_0$ (these amplitudes are indicated by circles in figure 2). It is common to quote the ratio between the width of the islands and the distance between the rational surfaces (the so-called Chirikov overlap parameter) as a measure of the level of stochasticity. This parameter is also shown in figure 2.

For sufficiently high amplitudes ($\psi_0 \geqslant 6.5$), the perturbation (5) leads to a stabilization of the barrier relaxations (figure 3 (left, middle and bottom)). Except for very high perturbation amplitudes ($\psi_0 \geqslant 19$), the control of barrier relaxations is accompanied by only a slight degradation of the energy confinement time (figure 3 (right)). This behavior can be attributed to an erosion of the transport barrier and a steepening of the pressure gradient next to the barrier (on the outward side) [15, 16], as can be seen from figure 4(*a*).

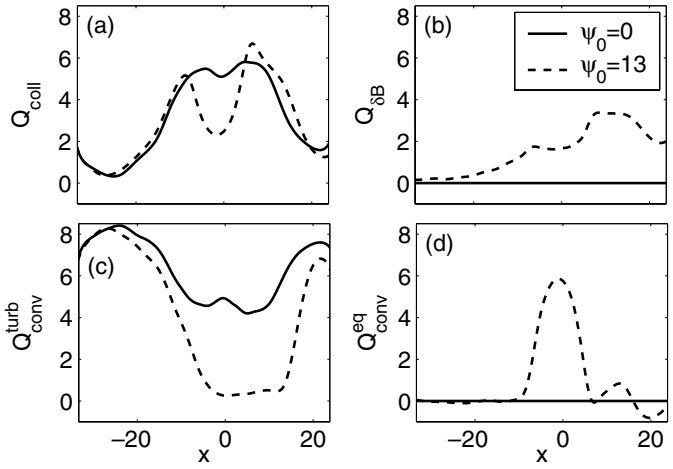

Figure 4. Radial profiles of the different contributions to the energy flux balance (4), with and without the multiple harmonics magnetic perturbation (5). According to (6) and (7), the convective flux is decomposed into two parts, one associated with the equilibrium and one associated with fluctuations. Parameters are the same as in figure 3.

Although the radial energy flux $Q_{\delta B}$, i.e. the radial component of the collisional parallel heat flux on perturbed magnetic surfaces, is increasing with the perturbation amplitude ψ_0 (figure 4(*b*)), the erosion of the transport barrier is mainly caused by the convective flux

$$Q^{\mathrm{eq}}_{\mathrm{conv}} = \left\langle p^{\mathrm{eq}} \partial_y \phi^{\mathrm{eq}} \right\rangle_{y,z} \tag{6}$$

associated with the non-axisymmetric plasma equilibrium in the presence of the magnetic perturbation. Here

$$p^{\mathrm{eq}}(x, y, z) = \langle p \rangle_t , \qquad \phi^{\mathrm{eq}}(x, y, z) = \langle \phi \rangle_t ,$$

where $\langle \cdot \rangle_t$ is the time average in a statistically stationary state [23]. The convective energy flux associated with fluctuations,

$$Q^{\mathrm{turb}}_{\mathrm{conv}} = Q_{\mathrm{conv}} - Q^{\mathrm{eq}}_{\mathrm{conv}}, \tag{7}$$

is decreasing with the perturbation amplitude ψ_0 (figure 4(*c*)), but the convective flux associated with the equilibrium $Q^{\mathrm{eq}}_{\mathrm{conv}}$ is strongly increasing, especially in the barrier center (figure 4(*d*)), where residual islands are present even for high perturbation amplitudes ψ_0 (when field line stochastization occurs between the barrier and the outer plasma edge) [15, 16].

3.2. Single harmonic perturbation

As the stabilization of barrier relaxations is mainly due to an erosion of the barrier associated with a magnetic island chain localized at the barrier position, we expect a similar effect when restricting the perturbation (5) to the single harmonic that is resonant at $q = 3$,

$$\psi^{\mathrm{single}}_{\mathrm{RMP}} = \psi_0 \psi_{m_0}(x) \cos\left(m_0\theta - n_0\varphi\right) \qquad \text{with} \quad \psi_{m_0}(x) = \exp\left(\frac{m_0 \xi_{\mathrm{bal}}}{\beta_1 r_{\mathrm{c}}} x\right). \tag{8}$$

This magnetic perturbation is indeed stabilizing the barrier relaxations (figure 5 (left, middle and bottom)), however, even for relatively low perturbation amplitudes ψ_0, this stabilization is accompanied by a significant reduction in the edge energy confinement time (figure 5 (right)). In fact, as shown in figure 6(*a*), the erosion at the barrier center is similar compared with the

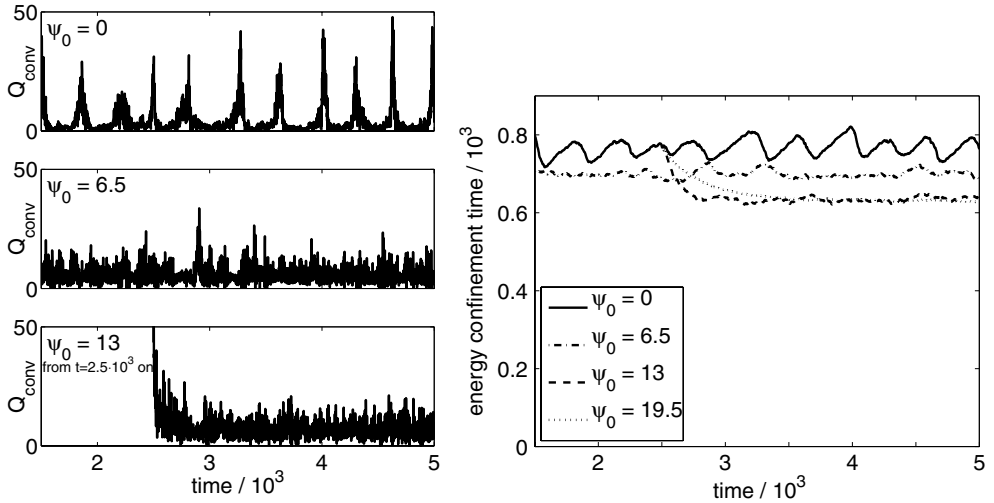

Figure 5. Time evolutions of the convective flux Q_{conv} at the barrier center $x = 0$, $q = 3$ (left) and of the edge energy confinement time (right) for different amplitudes ψ_0 of the single harmonic magnetic perturbation (8). Parameters are the same as in figure 3.

one observed with the multiple harmonics perturbation, but the single harmonic perturbation does not affect the pressure profile far from its resonant surface. In particular, the steepening of the pressure gradient between the barrier and the outer edge, observed in the case of the multiple harmonics perturbation, and compensating for the erosion of the barrier, is not present in the case of the single harmonics perturbation [17]. In both cases, however, the erosion of the transport barrier is mainly due to the convective flux $Q_{\mathrm{conv}}^{\mathrm{eq}}$ associated with the helical plasma equilibrium induced by the magnetic island chain (figures 4(*d*) and 6(*d*)). In the following section, we further analyze the properties of this transport.

4. Convective transport in non-axisymmetric equilibrium with magnetic islands

In order to study the non-axisymmetric equilibrium in the presence of the single harmonic magnetic perturbation (8), we run the turbulence code for low values of the total energy flux Q_{tot} such that the resulting pressure gradient $\kappa = Q_{\mathrm{tot}}/\chi_\perp$ is below the threshold for resistive ballooning instability. The three-dimensional pressure and electric potential fields then evolve to a stationary state corresponding to the equilibrium. In order to get some analytic insight into the structure of this equilibrium and the associated transport, we study the case of cylindrical magnetic curvature only, i.e. the operator $\boldsymbol{G}$ is replaced by $\boldsymbol{G} = g_0\partial_y$. (Here the average curvature parameter $g_0 = 0.7$ is chosen such that resistive ballooning modes remain stable for the same value of the total flux Q_{tot} mentioned above). In this case, only mode numbers that are multiples of (m_0, n_0) contribute to the pressure and potential equilibrium in the presence of the magnetic perturbation with mode number (m_0, n_0). Furthermore, the numerical results show that the amplitudes of the higher order harmonics $(2m_0, 2n_0)$, $(3m_0, 3n_0)$, ... are lower by at least a factor of 10^{-2} compared with the main harmonic. Neglecting the higher order harmonics, the equilibrium pressure and potential can be written as

$$\begin{pmatrix} p^{\mathrm{eq}} \\ \phi^{\mathrm{eq}} \end{pmatrix} = \begin{pmatrix} \bar{p}(x) \\ \bar{\phi}(x) \end{pmatrix} + \begin{pmatrix} p_1(x) \\ \phi_1(x) \end{pmatrix} \mathrm{e}^{\mathrm{i}(m_0\theta - n_0\varphi)} \,. \tag{9}$$

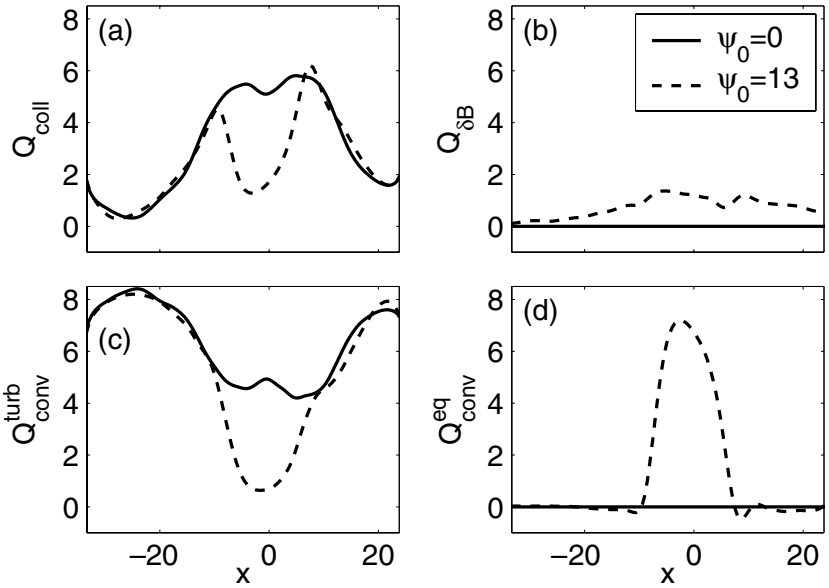

Figure 6. Radial profiles of the different contributions to the energy flux balance (4), with and without the single harmonics magnetic perturbation (8). According to (6) and (7), the convective flux is decomposed into two parts, one associated with the equilibrium and one associated with fluctuations. Parameters are the same as in figure 3. The island width corresponding to the perturbation amplitude $\psi_0 = 13$ is $W = 14.4$. We recall the shear layer width $d = 11.7$.

Inserting the expressions (8), (9) in (1), (2) reveals that $\bar{p}$, $\bar{\phi}$, p_1 and ϕ_1 are determined by the following set of equations:

$$2k_y\partial_x\Im\left(\phi_1 p_1^*\right) = -2\chi_\parallel k_y^2\partial_x\left(x\psi_1\Re p_1 - \psi_1^2\partial_x\bar{p}\right) + \chi_\perp\partial_x^2\bar{p} + S, \tag{10}$$

$$-\frac{1}{2}k_y\partial_x\Im\left[\phi_1\left(\partial_x^2 - k_y^2\right)\phi_1^*\right] = 2k_y^2\partial_x\left(x\psi_1\Re\phi_1 - \psi_1^2\partial_x\bar{\phi}\right) + \nu\partial_x^4\bar{\phi} + \mu\partial_x^2\left(\phi_{\rm imp} - \bar{\phi}\right), \tag{11}$$

$$\begin{aligned}\frac{\mathrm{i}}{k_y}\left(p_1\partial_x\bar{\phi} - \phi_1\partial_x\bar{p}\right) = {}& \frac{\mathrm{i}}{k_y}\delta_{\rm c}g_0\phi_1 - \chi_\parallel x^2 p_1 + \chi_\parallel x\psi_1\partial_x\bar{p} + 2\mathrm{i}\chi_\parallel\psi_1\partial_x^2\left(\psi_1\Im p_1\right)\\ & + \chi_\parallel\left(\psi_1\partial_x - 2\partial_x\psi_1\right)\partial_x\left(\psi_1 p_1\right) + \frac{\chi_\perp}{k_y^2}\left(\partial_x^2 - k_y^2\right)p_1,\end{aligned} \tag{12}$$

$$\begin{aligned}\frac{\mathrm{i}}{k_y}\left[\partial_x\bar{\phi}\left(\partial_x^2 - k_y^2\right)\phi_1 - \phi_1\partial_x^3\bar{\phi}\right] = {}& -\frac{\mathrm{i}}{k_y}g_0 p_1 + x^2\phi_1 - x\psi_1\partial_x\bar{\phi} - 2\mathrm{i}\psi_1\partial_x^2\left(\psi_1\Im\phi_1\right)\\ & - \left(\psi_1\partial_x - 2\partial_x\psi_1\right)\partial_x\left(\psi_1\phi_1\right) + \frac{\nu}{k_y^2}\left(\partial_x^2 - k_y^2\right)^2\phi_1,\end{aligned} \tag{13}$$

where $\psi_1(x) = \psi_0\psi_{m_0}(x)/2$ and $k_y = m_0\xi_{\rm bal}/r_0$. Note that by radially integrating the transport equation (10), one recovers the energy flux balance (4) with

$$Q^{\rm eq}_{\rm conv} = 2k_y\Im\left(\phi_1 p_1^*\right) \qquad \text{and} \qquad Q^{\rm eq}_{\delta B} = 2\chi_\parallel k_y^2\psi_1\left(x\Re p_1 - \psi_1\partial_x\bar{p}\right). \tag{14}$$

Analytical expressions for parts of the radial profiles $p_1(x)$ and $\phi_1(x)$ can be obtained in the *constant-ψ approximation*, i.e. when neglecting the radial variation of the magnetic perturbation amplitude by assuming $\psi_1(x) = \text{const} = \psi_1(0) = \psi_0/2$. In this case, the width W of the magnetic islands induced by the perturbation is given by $W = 4\sqrt{\psi_0}$ and the ratio of

$\chi_\perp$ to $\chi_\parallel$ gives rise to a critical island width $W_c = (8/k_y)^{1/2}(\chi_\perp/\chi_\parallel)^{1/4}$ [7]. In the constant-ψ approximation, the last two terms in (12) can be combined to form an effective perpendicular dissipation

$$\chi_\parallel \psi_1^2 \partial_x^2 p_1 + \frac{\chi_\perp}{k_y^2}\left(\partial_x^2 - k_y^2\right) p_1 = \frac{\chi_\perp}{k_y^2}\left\{\left[\left(\frac{W}{2W_c}\right)^4 + 1\right]\partial_x^2 - k_y^2\right\} p_1.$$

Far from the resonance layer, i.e. for $|x| \gg W$, this perpendicular dissipation can be neglected and analytical expressions for $\bar{p}$, $\bar{\phi}$, p_1 and ϕ_1 can be obtained when no poloidal rotation is imposed ($\mu = 0$). Let us first study this case (i.e. in the absence of a transport barrier).

4.1. Case with no imposed rotation

In this case, with the constant-ψ approximation and for $|x| \gg W$ (neglecting perpendicular dissipation), a solution of system (10)–(13) is given by

$$\bar{p} = -\kappa\,(x - x_{\max})\,, \qquad \bar{\phi} = 0, \tag{15}$$

$$p_1 = -g(x)\kappa\frac{\psi_0}{2}\frac{1}{x}, \qquad \phi_1 = -\mathrm{i}g(x)\frac{g_0\kappa}{k_y}\frac{\psi_0}{2}\frac{1}{x^3}\,, \tag{16}$$

$$\text{with } \kappa = \frac{Q_{\mathrm{tot}}}{\chi_\perp}, \quad g(x) = \left[1 - \left(\Gamma\frac{W_c}{x}\right)^4\right]^{-1}, \quad \Gamma = \left[\frac{g_0\,(\kappa - \delta_c g_0)}{64\chi_\perp}\right]^{\frac{1}{4}}$$

where we have assumed that the fluxes $Q_{\mathrm{conv}}^{\mathrm{eq}}$ and $Q_{\delta B}$ are small compared with Q_{coll} such that the pressure gradient κ is given by $Q_{\mathrm{tot}}/\chi_\perp$. Obviously, this is not true in the simulations with turbulence presented in section 3. However, the assumption is verified when the total energy flux is below the instability threshold, as we will show *a posteriori*. The second term in the expressions for $g(x)$ can be neglected for $|x| \gg \Gamma W_c$. Therefore, sufficiently far from the resonant surface, the solutions for p_1 and ϕ_1 write

$$p_1 = -\kappa\frac{\psi_0}{2}\frac{1}{x}, \quad \phi_1 = -\mathrm{i}\frac{g_0\kappa}{k_y}\frac{\psi_0}{2}\frac{1}{x^3} \qquad \text{for} \quad |x| \gg \max\left(\Gamma W_c, W\right) \tag{17}$$

The solution for p_1 is identical to the expression given in [7] for the profile of the helical pressure variation far from the resonant surface. It arises from the parallel and perpendicular diffusion terms in the pressure equation (12). Far from the resonant surface, this solution is determined by the balance between the two main terms coming from the parallel diffusion $\chi_\parallel \nabla_\parallel^2 p$ (the second and third term on the rhs). In addition, the coupling between pressure and potential induced by the magnetic curvature in the charge balance (13) (far from the resonance: the balance between the first and second term on the rhs) leads to a non-vanishing helical potential variation ϕ_1. The numerical results for the profiles p_1 and ϕ_1 and a comparison with the solution (17) are presented in figure 7. The pressure variation corresponds to a (weak) flattening of the pressure gradient on the magnetic islands. The potential variation is phase shifted by $\pi/2$ with respect to the pressure variation and corresponds to stationary convection cells, one on each side of an island.

A similar potential structure has recently been observed in a two-dimensional Hasegawa–Wakatani model in the presence of a magnetic island [24]. However, in this model, a strong mean poloidal flow is present in addition to the helical flow variation such that the total flow structure is more complex then convection cells. In this study, no poloidal mean flow is generated in the equilibrium with magnetic islands (see (15)). This is consistent with the fact that the potential variation ϕ_1 is purely imaginary, as can be seen from (11) (both, the Reynolds stress on the lhs as well as the $\Re\phi_1$ term on the rhs vanish). We will come back to the relation

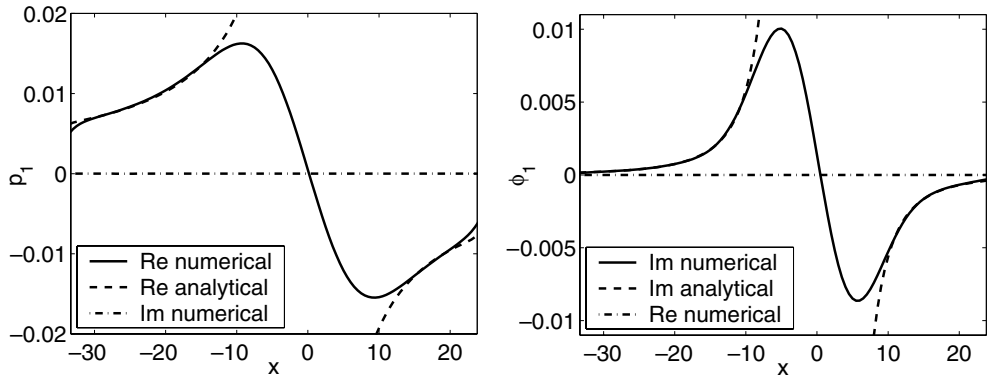

Figure 7. Radial profiles of the non-axisymmetric components of pressure and potential in an equilibrium with magnetic island in a case without imposed poloidal rotation. Here, $Q_{\rm tot} = 0.1$, $\psi_0 = 3.9$ ($W = 7.9$).

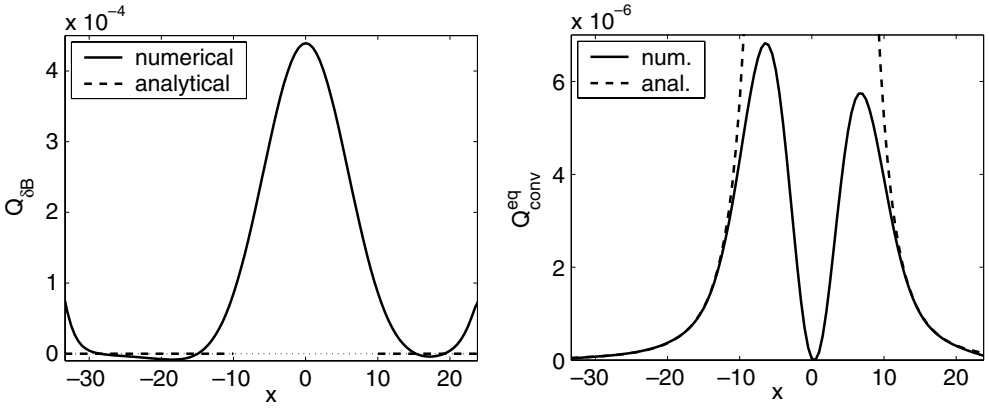

Figure 8. Radial profiles of the radial energy flux due to the parallel diffusion $Q_{\delta B}$ and the convective flux associated with the non-axisymmetric equilibrium $Q^{\rm eq}_{\rm conv}$ in the case without imposed poloidal rotation. Parameters are the same as in figure 7.

between the real part of the potential variation ϕ_1 and the mean poloidal flow when studying the case with imposed flow in the next subsection.

When inserting the solution (17) in expressions (14) for $Q^{\rm eq}_{\rm conv}$ and $Q_{\delta B}$, it becomes obvious that the phase shift of $\pi/2$ between the helical pressure and potential variations leads to a non-vanishing convective flux $Q^{\rm eq}_{\rm conv}$ associated with the equilibrium. This flux increases as $1/x^4$ when approaching the resonance surface. The radial flux due to the parallel diffusion $Q_{\delta B}$ is vanishing far from the resonant surface,

$$Q^{\rm eq}_{\rm conv} = g_0 \kappa^2 \frac{\psi_0^2}{2} \frac{1}{x^4}, \quad Q_{\delta B} = 0 \qquad \text{for} \quad |x| \gg \max\left(\Gamma W_{\rm c}, W\right).$$

These solutions and the numerical results for the complete profiles are shown in figure 8. Note that the flux $Q_{\delta B}$ is calculated here by an average over unperturbed flux surfaces (i.e. over the poloidal and toroidal angles). This approach is justified for the set of parameters used in our study, i.e. $W = 7.9$, $W_{\rm c} = 17.9$, $\Gamma W_{\rm c} = 3.3$, corresponding to small islands where

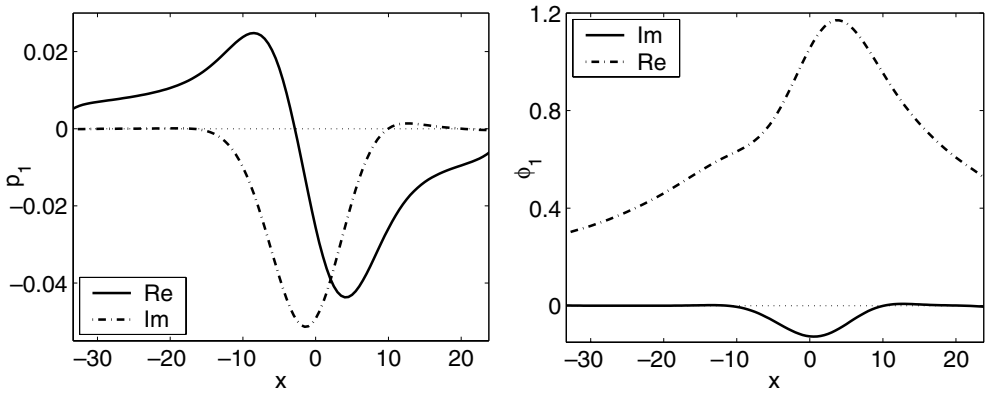

Figure 9. Radial profiles of the non-axisymmetric components of pressure and potential in an equilibrium with magnetic island in a case with imposed poloidal rotation. Parameters are the same as in figure 7 and $\mu = 2$, $\omega_E = 0.5$, $d = 11.7$.

perpendicular transport competes with parallel fluxes along the perturbed field lines. For large perturbations, parallel transport fluxes dominate and averages along the island's flux surfaces are necessary in order to evaluate the smaller transport fluxes across magnetic surfaces. Note also that from expressions (14) and (16) it is obvious that the flux $Q_{\delta B}$ is finite only for a non zero pressure gradient κ. The latter is determined by perpendicular heat transport which therefore is critical for a finite flux $Q_{\delta B}$.

4.2. Case with imposed rotation

We now come back to the case that is of particular interest for the understanding of the modification of the transport barrier in section 3. When a mean poloidal rotation $\partial_x \bar{\phi}$ is imposed, a non-vanishing real part of the potential variation ϕ_1 is induced by the balance of the two main terms in the parallel divergence of the parallel current $\nabla_\parallel^2 \phi$ in the charge balance (13) (second and third term on the rhs). This is equivalent to the generation of the (real part of the) pressure variation p_1 (17) by the coupling to the pressure gradient $\partial_x \bar{p}$ (balance of the two main terms in the parallel diffusion $\chi_\parallel \nabla_\parallel^2 p$). Note that the perturbations described by the real parts of p_1 and ϕ_1 are in phase with the magnetic flux perturbation ψ_{RMP}.

However, in contrast to the pressure gradient $\partial_x \bar{p}$ which is approximatively constant here, the poloidal rotation $\partial_x \bar{\phi}$ is an odd function of the radial coordinate x (see figure 2 (top)). Therefore, the real part of the potential variation ϕ_1 is approximatively an even function, as well as the imaginary part of the pressure variation p_1 that is generated as before by the coupling between potential and pressure due to the magnetic curvature. The profiles of these variations are shown in figure 9. They give rise now to a convective flux $Q_{\mathrm{conv}}^{\mathrm{eq}}$ associated with the helical equilibrium that presents a maximum on the resonant surface and that has a significantly higher amplitude than the radial flux $Q_{\delta B}$ due to the parallel diffusion (figure 10). The qualitative findings concerning the importance of the convective flux associated with the non-axisymmetric equilibrium agree well with the observations in section 3 revealing that this flux plays an important role in the erosion of the transport barrier and the subsequent stabilization of barrier relaxations.

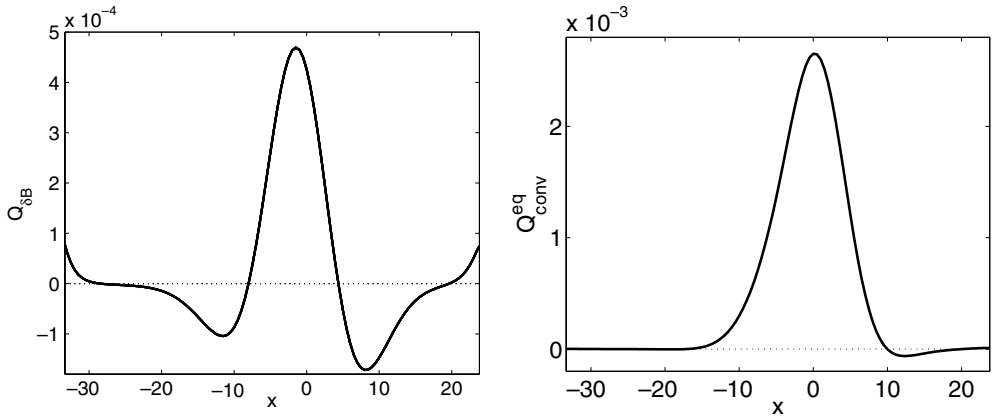

Figure 10. Radial profiles of the radial energy flux $Q_{\delta B}$ due to the parallel diffusion and the convective flux $Q^{\mathrm{eq}}_{\mathrm{conv}}$ associated with the non-axisymmetric equilibrium in the case with imposed poloidal rotation. Parameters are the same as in figure 9.

5. Conclusions

Transport barrier relaxation oscillations observed in three-dimensional turbulence simulations can be controlled by multiple harmonics or single harmonic RMPs. This stabilization is due to an erosion of the barrier. In the first geometry, for intermediate perturbation amplitudes, the erosion of the barrier is compensated for by an increase in the pressure gradient outside the barrier, and the overall confinement is nearly unchanged. The single harmonics RMP always leads to a degradation of the confinement. The barrier erosion is due to an enhanced radial energy flux in the presence of magnetic islands. Two different mechanisms are at the origin of this enhancement. One is the radial energy flux due to the collisional heat transport along perturbed magnetic field lines. The second is a convective flux associated with the non-axisymmetric equilibrium in the presence of the magnetic island. When a sheared poloidal rotation of the plasma is present—that is at the origin of the transport barrier—the equilibrium convective flux is found to be more important than the radial component of the flux along the field lines.

References

[1] Connor J W 1998 *Plasma Phys. Control. Fusion* **40** 531
[2] Evans T E *et al* 2004 *Phys. Rev. Lett.* **92** 235003
[3] Burrell K H *et al* 2005 *Plasma Phys. Control. Fusion* **47** B37
[4] Liang Y *et al* 2007 *Phys. Rev. Lett.* **98** 265004
[5] Finken K H *et al* 2007 *Nucl. Fusion* **47** 522
[6] Unterberg B *et al* 2009 *J. Nucl. Mater.* **390–391** 351
[7] Fitzpatrick R 1995 *Phys. Plasmas* **2** 825
[8] Bécoulet M *et al* 2005 *Nucl. Fusion* **45** 1284
[9] Nardon E, Bécoulet M, Huysmans G and Czarny O 2007 *Phys. Plasmas* **14** 092501
[10] Bécoulet M *et al* 2009 *Nucl. Fusion* **49** 085011
[11] Waelbroeck F L 2003 *Phys. Plasmas* **10** 4040
[12] Heyn M F *et al* 2008 *Nucl. Fusion* **48** 024005
[13] Beyer P *et al* 2005 *Phys. Rev. Lett.* **94** 105001
[14] Beyer P *et al* 2007 *Plasma Phys. Control. Fusion* **49** 507
[15] Leconte M, Beyer P, Garbet X and Benkadda S 2009 *Phys. Rev. Lett.* **102** 045006

[16] Leconte M, Beyer P, Garbet X and Benkadda S 2010 *Nucl. Fusion* **50** 054008
[17] de Solminihac F *et al* 2010 *Contrib. Plasma Phys.* **50** 343
[18] Scott B D 1997 *Plasma Phys. Control. Fusion* **39** 1635
[19] Beyer P, Benkadda S and Garbet X 2000 *Phys. Rev.* E **61** 813
[20] Figarella C F, Benkadda S, Beyer P, Garbet X and Voitsekhovich I 1993 *Phys. Rev. Lett.* **90** 015002
[21] Abdullaev S S, Finken K H, Jakubowski M W, Kasilov S V, Kobayashi M, Reiser D, Runov M A and Wolf R 2003 *Nucl. Fusion* **43** 299
[22] Haberscheidt T 2006 *PhD Thesis* University of Bochum
[23] Beyer P, Garbet X, Benkadda S, Ghendrih P and Sarazin Y 2002 *Plasma Phys. Control. Fusion* **44** 2167
[24] Waelbroeck F L, Militello F, Fitzpatrick R and Horton W 2009 *Plasma Phys. Control. Fusion* **51** 015015